Computer Aided Diagnosis system for prostatic biopsy guidance and follow-up fusing multi-modal imaging.

Guillaume Lemaître

LE2I - ViCOROB

Université de Bourgogne - Universitat de Girona

Supervisors:

Jordi Freixenet Bosch (ViCOROB - UdG)

Fabrice Mériaudeau (CISIR - UTP)

Robert Marí Marly (ViCOROB - UdG)

Paul Michael Walker (LE2I - UBFC)

A thesis submitted for the degree of

PhilosophiæDoctor (PhD)

April 2015

1. Reviewer: Name

2. Reviewer:

Day of the defense:

Signature from head of PhD committee:

Abstract

Put your abstract or summary here, if your university requires it.

To ...

Acknowledgements

I would like to acknowledge the thousands of individuals who have coded for the LaTeX project for free. It is due to their efforts that we can generate professionally typeset PDFs now.

Contents

List of Abbreviations

ADC apparent diffusion coefficient

BPH benign prostatic hyperplasia

CAD computer-aided detection and diangosis

CADe computer-aided detection

CADx computer-aided diagnosis

CaP prostate cancer

CG central gland

Chap. Chapter

CSE chemical shift effect

CZ central zone

DCE dynamic contrast-enhanced

DW diffusion weighted

EES extravascular-extracellular space

Eq. equation

ERSSPC European Randomized Study of Screening for Prostate Cancer

Fig. figure

FSE Fast Spin-Echo

GS Gleason score

MRI magnetic resonance imaging

MRSI magnetic resonance spectroscopy imaging

NMR nuclear magnetic resonance

PLCO Prostate Lung Colorectal and Ovarian

PSA prostate-specific antigen

PZ peripheral zone

Sect. section

SI signal intensity

SNR signal-to-noise

T_2-W T_2 Weighted

TE echo time

TR repetition time

TRUS transrectal ultrasound

TZ transitional zone

US ultrasound

List of Figures

List of Tables

Chapter 1

Introduction

1.1 Prostate anatomy

The prostate is an exocrine gland of the male reproductive system having an inverted pyramidal shape, which is located below the bladder and infront of the rectum (see Fig. 1.1). It measures approximately three centimetres in height by two and half centimetres in depth and its weight is estimated to be between seven and sixteen grams for an adult (2)). The prostate size increases at two distinct stages during physical development: initially at puberty to reach its normal size, then again after sixty years of age leading to benign prostatic hyperplasia (BPH) (3)).

A zonal classification of the prostate, depicted in Fig. 1.2, was suggested by McNeal (4)). Subsequently, this categorization was widely accepted in the literature (cf., (3,

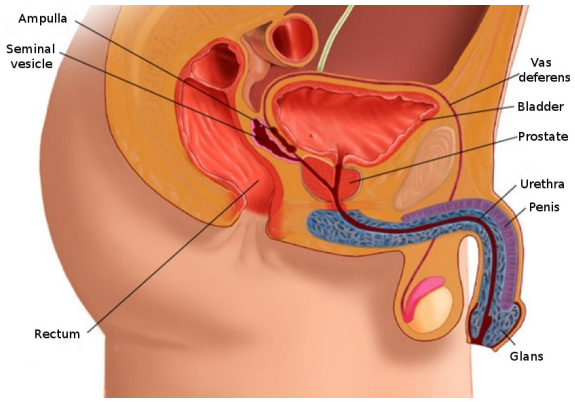

Figure 1.1: Sagittal anatomy scheme of the male reproductive system.

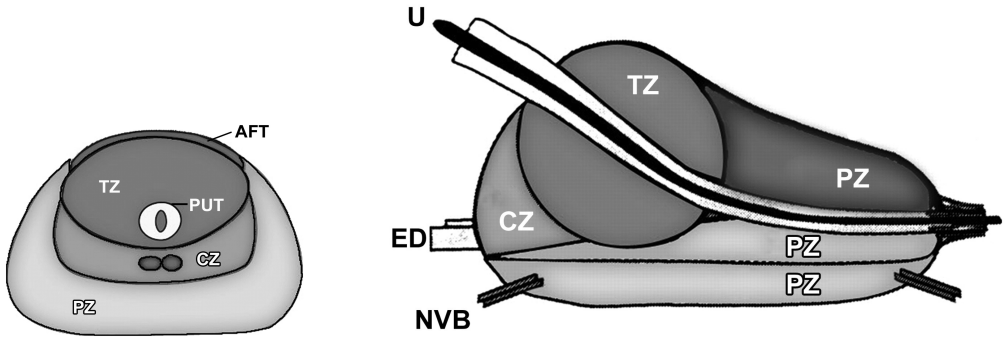

(a) Transverse anatomy of the prostate.

(b) Sagittal anatomy of the prostate.

Figure 1.2: Prostate anatomy with division in different zones. *AFT:* anterior fibromuscular tissue, *CZ:* central zone, *ED:* ejaculatory duct, *NVB:* neurovascular bundle, *PUT:* tissue, *PZ:* peripheral zone, *U:* urethra, *TZ:* transitional zone, *B:* base, *M:* median, *A:* apex (copyright by (1)).

5, 6, 7)) and is used in all medical examinations (e.g., biopsy, MRI screening). The classification is based on dividing the gland into three distinct regions: (i) central zone (CZ) accounting for 20-25% of the whole prostate gland, (ii) transitional zone (TZ) standing for 5% and (iii) peripheral zone (PZ) representing the 70%. In MRI images, tissues of CZ and TZ are difficult to distinguish and are usually merged into a common region, denominated central gland (CG). As part of this classification, the prostate can be divided in three longitudinal portions depicted in Fig. 1.2(b): (i) base, (ii) median gland and (iii) apex.

1.2 Prostate carcinoma

Prostate cancer (CaP) has been reported on a worldwide scale to be the second most frequently diagnosed cancer of men accounting for 13.6% (8). Statistically, in 2008, the number of new diagnosed cases was estimated to be $899,000$ with no less than $258,100$ deaths (8). In United States, aside from skin cancer, CaP was declared to be the most commonly diagnosed cancer among men, implying that approximately one in six men will be diagnosed with CaP during their lifetime and one in thirty-six will die from this disease causing CaP to be the second most common cause of cancer death among men

(9), (10).

Despite active research to determine the causes of prostate cancer, a fuzzy list of risk factors has arisen (11). The etiology was linked to the following factors (11): (i) family history (12, 13), (ii) genetic factors (14, 15, 16), (iii) race-ethnicity (12, 17), (iv) diet (12, 18, 19), and (v) obesity (12, 20). This list of risk factors alone cannot be used to diagnose CaP and in this way, screening enables early detection and treatment.

CaP growth is characterized by two main types of evolution (21): slow-growing tumours, accounting for up to 85 % of all CaPs (22), progress slowly and usually stay confined to the prostate gland. For such cases, treatment can be substituted with active surveillance. In contrast, the second variant of CaPs develops rapidly and metastasises from prostate gland to others organs, primarily the bones (23). Bone metastases, being an incurable disease, significantly affects the morbidity and mortality rate (24). Hence, the results of the surveillance have to be trustworthy in order to distinguish aggressive from slow-growing CaP.

CaP is more likely to come into being in specific regions of the prostate. In that respect, around 70-80 % of CaPs originate in PZ whereas 10-20 % in TZ (25, 26, 27). Only about 5 % of CaPs occur in CZ (26, 28). However, those cancers appear to be more aggressive and more likely to invade other organs due to their location (28).

1.3 CaP screening and imaging techniques

Current CaP screening consists of three different stages. First, prostate-specific antigen (PSA) control is performed to distinguish between low and high risk CaP. Then, for confirmation, samples are taken during prostate biopsy and finally analysed to evaluate the prognosis and the stage of CaP. In this section, we present a detailed description of the current screening as well as its drawbacks.

Since its introduction in mid-1980s, PSA is widely used for CaP screening (29). A higher-than-normal level of PSA can indicate an abnormality of the prostate either as a BPH or a cancer (30). However, other factors can lead to an increased PSA level such as prostate infections, irritations, a recent ejaculation or a recent rectal examination (3). PSA can be found in the bloodstream in two different forms: free PSA (about 10%), and linked to another protein (about 90%). A level of PSA higher than 10 $ng.mL^{-1}$ is considered to be at risk (3). If the PSA level is between 10 $ng.mL^{-1}$ and 4 $ng.mL^{-1}$,

the patient is considered as suspicious (31). In that case, the ratio of free PSA to total PSA is computed; if the ratio is higher than 15%, the case is considered as pathological (3).

A transrectal ultrasound (TRUS) biopsy is carried out for cases which are considered as pathological. At least six different samples are taken randomly from the right and left parts of three different zones: apex, median and base. These samples are further evaluated using the Gleason grading system (32). The scoring scheme to characterize the biopsy sample is composed of five different patterns which correspond to grades ranging from 1 to 5. Higher grades are associated with poor prognosis (33). Then, in the Gleason system, two scores are assigned corresponding to (i) the grade of the most present tumour pattern, and (ii) the grade of the second most present tumour pattern (33). A higher GS indicates a more aggressive tumour (33). Also, it should be noted that biopsy is an invasive procedure which can result in serious infection or urine retention (34, 35).

Although PSA screening has been shown to improve early detection of CaP (35), its lack of reliability motivates further investigations using MRI-CAD. Two reliable studies, carried out in the United States (36) and in Europe (37, 38), have attempted to assess the impact of early detection of CaP, with diverging outcomes (35, 39). The study carried out in Europe[1] concluded that PSA screening reduces CaP-related mortality by 21-44% (37, 38), while the American[2] trial found no such effect (36). However, both studies agree that PSA screening suffers from low specificity, with an estimated rate of 36 % (40). Both studies also agree that over-treatment is an issue: decision making regarding treatment is further complicated by difficulties in evaluating the aggressiveness and progression of CaP (41).

Hence, new screening methods should be developed with improved specificity of detection as well as more accurate risk assessment (aggressiveness and progression). Current research is focused on identifying new biological markers to replace PSA-based screening (42, 43, 44). Until such research comes to fruition, these needs can be met through active-surveillance strategy using multi-parametric MRI techniques (30, 45).

[1]The European Randomized Study of Screening for Prostate Cancer (ERSSPC) started in the 1990s in order to evaluate the effect of PSA screening on mortality rate.

[2]The Prostate Lung Colorectal and Ovarian (PLCO) cancer screening trial is carried out in the United States and intends to ascertain the effects of screening on mortality rate.

An MRI-CAD system, which is an area of active research and forms the focus of this thesis, can be incorporated into this screening strategy allowing a more systematic and rigorous follow-up.

Another weakness of the current screening strategy lies in the fact that TRUS biopsy does not provide trustworthy results. Due to its "blind" nature, there is a chance of missing aggressive tumours or detecting microfocal "cancers", which influences the aggressiveness-assessment procedure (46). As a consequence, over-diagnosis is estimated at up to 30 % (47), while missing clinically significant CaP is estimated at up to 35 % (48). In an effort to solve both issues, alternative biopsy approaches have been explored. MRI/ultrasound (US)-guided biopsy has been shown to outperform standard TRUS biopsy (49). There, multimodal MRI images are fused with US images in order to improve localization and aggressiveness assessment to carry out biopsies. Human interaction plays a major role in biopsy sampling which can lead to low repeatability; by reducing potential human errors at this stage, the CAD framework can be used to improve repeatability of examination. CaP detection and diagnosis benefit from the use of CAD and MRI techniques.

In an effot to improve the current statge of CaP diagnosis and detection, this thesis is intended to provide a multiparameteric MRI CAD system. MRI principles and its different modalites are presented in Chapter (Chap.) 2.

1.4 Computer-aided systems for CaP

During the last century, physicists have focused on constantly innovating in terms of imaging techniques assisting radiologists to improve cancer detetction and diagnosis. However, human diagnosis still suffers from low repeatability, synonymous with erroneous detection or interpretations of abnormalities throughout clinical decisions (50, 51). These errors are driven by two majors causes (50): observer limitations (e.g., constrained human visual perception, fatigue or distraction) and the complexity of the clinical cases themselves, for instance due to unbalanced data (number of healthy cases more abundant than malignant cases) or overlapping structures.

Computer vision has given rise to many promising solutions, but, instead of focusing on fully automatic computerized systems, researchers have aimed at providing computer image analysis techniques to aid radiologists in their clinical decisions (50). In fact,

these investigations brought about both concepts of computer-aided detection (CADe) and computer-aided diagnosis (CADx) grouped under the acronym CAD. Since those first steps, evidence has shown that CAD systems enhance the diagnosis performance of radiologists. Chan *et al.* reported a significant 4 % improvement in breast cancer detection (52), which has been confirmed in later studies (53). Similar conclusions were drawn in the case of lung nodule detection (54), colon cancer (55) and CaP as well (51). Chan *et al.* (52) also hypothesized that CAD systems will be even more efficient assisting inexperienced radiologists than senior radiologists. That hypothesis was tested by Hambrock *et al.* (51) and was confirmed in case of CaP detection. In this particular study, inexperienced radiologists obtained equivalent performance to senior radiologists, both using CAD whereas the accuracy of their diagnosis was significantly poorer without CAD's help.

In contradiction with the aforementioned statement, CAD for CaP is a young technology due to the fact that is based on MRI (56). Four distinct MRI modalities are employed in CaP diagnosis which were mainly developed after the mid-1990s: (i) T_2-W MRI (57), (ii) DCE MRI (58), (iii) MRSI (59) and (iv) DW MRI (60). In addition, the increase of magnetic field strength (from 1.5 to 3 Tesla) and the development of endorectal coils, both imporved image spatial resolution (61) needed to perform more accurate diagnosis. It is for this matter that the development of CAD for CaP is still lagging behind fields stated above.

This research is aimed at first, to provide an overview of the current state-of-the-art of CAD for CaP and later, according to the drawn coclusions, to propose a CAD which takes advantag of multiparameteric MRI modalities. A review of the current proposed CAD for CaP is presented in Chap. 3.

1.5 Research motivation

1.6 Thesis outline

Chapter 2

MRI Principles and Imaging Techniques

2.1 MRI principles

2.2 MRI imaging techniques

MRI provides promising imaging techniques to overcome the previous mentioned drawbacks. Unlike TRUS biopsy, MRI examination is a non-invasive protocol and has been shown to be the most acute and harmless technique available currently (62). In this section, we review different MRI techniques developed for CaP detection and diagnosis. Features strengthening each modality, will receive particular attention together with their drawbacks. Commonly, these features form the basis for developing analytic tools and automatic algorithms. However, we refer the reader to Sect.. **??** for more details on automatic feature detection methods since they are part and parcel of the CAD framework. Table 2.1 provides an overview of the following discussion.

2.2.1 T_2-W MRI

T_2-W MRI was the first MRI-modality used to perform CaP diagnosis using MRI (57). Nowadays, radiologists make use of it for CaP detection, localization and staging purposes. This imaging technique is well suited to render zonal anatomy of the prostate (31).

Table 2.1: Overview of the features associated with each MRI modality. Acronyms: prostate cancer (CaP) - signal intensity (SI) - Gleason score (GS).

Modality	Significant features	CaP	Healthy tissue	GS correlation
T_2-W MRI	SI	low-SI	intermediate to high-SI	+
T_2 map	SI	low-SI	intermediate to high-SI	+
DCE MRI	Semi-quantitative features:			
	– wash-in	faster	slower	0
	– wash-out	faster	slower	0
	– integral under the curve	higher	lower	0
	– maximum signal intensity	higher	lower	0
	– time-to-peak enhancement	faster	slower	0
	Quantitative features (Tofts' parameters):			
	– k_{ep}	higher	lower	0
	– K^{trans}	higher	lower	0
DW MRI	SI	higher-SI	lower-SI	+
ADC map	SI	low-SI	high-SI	+
MRSI	Metabolites:			
	Citrate (2.64 ppm)	lower concentration	higher concentration	+
	Choline (3.21 ppm)	higher concentration	lower concentration	0
	Spermine (3.11 ppm)	lower concentration	higher concentration	+

Notes:
+ = significantly correlated.
0 = no correlation.

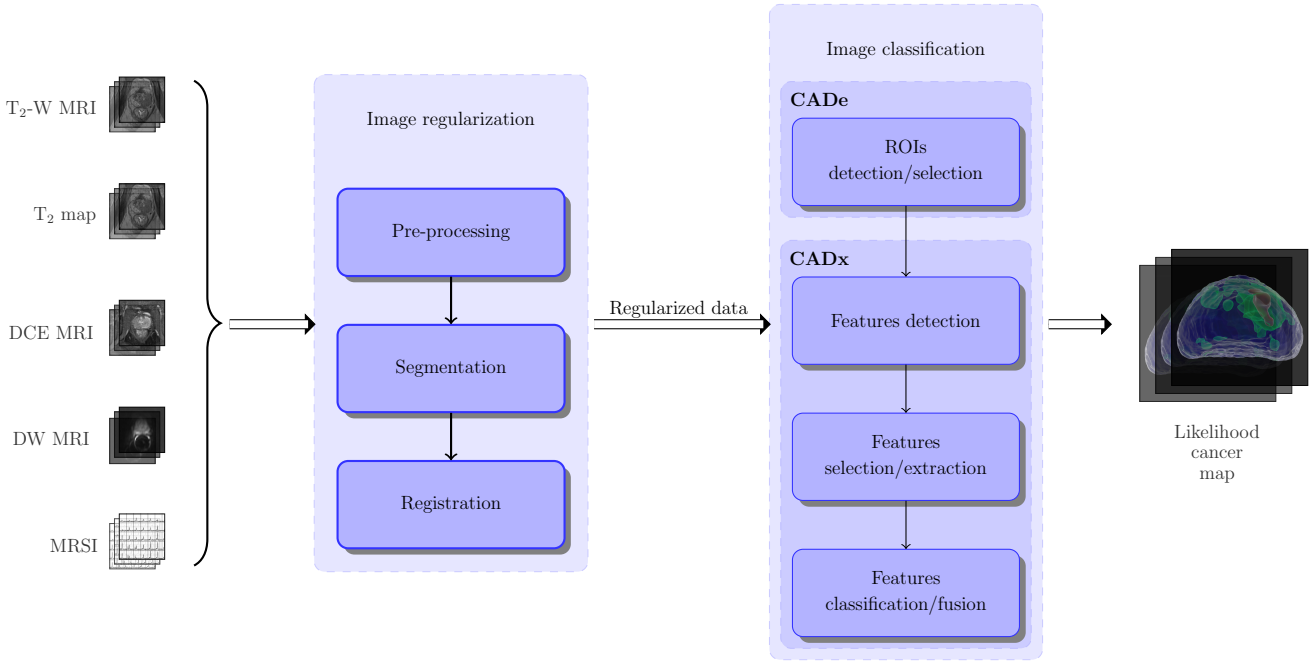

Figure 2.1: CAD framework using MRI images. Multiparametric MRI images are provided as inputs. These data arise from heterogeneous sources and need to be regularized. Some studies do not consider this stage as mandatory and do not implement or only partly those processes (see Tab. **??**). A pre-processing stage is usually applied to standardize the intensity of images, reduce noise and artefacts. Then, in the image set, the prostate organ has to be segmented to focus the next processing stages only on that particular ROI. Moreover, prostate location can vary depending of the modality chosen. Therefore, the images are registered so that all segmented images will be in the same reference frame. Once the image regularisation performed, image classification can be carried out. First, a strategy defining ROIs to focus on is decided. Then, distinctive features are extracted before to be post-processed to select the most salient features. Finally, these salient features will feed a classifier previously trained which will provide a likelihood cancer map associated with either CaP detection or diagnosis.

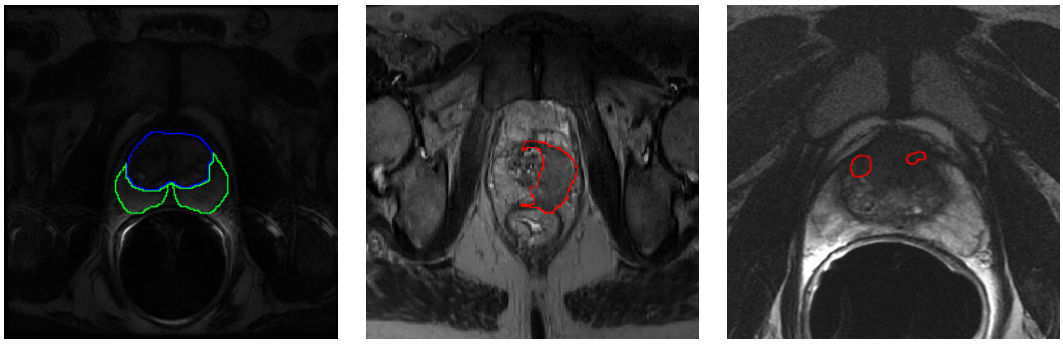

(a) T_2-W-MRI slice of an healthy prostate acquire with a 1.5 Tesla MRI. The blue contour represents the CG while the PZ corresponds to the green contour.

(b) T_2-W-MRI slice of a prostate with a CaP highlighted in the PZ using a 3.0 Tesla MRI scanner.

(c) T_2-W-MRI slice of a prostate with a CaP highlighted in the CG using a 3.0 Tesla MRI scanner.

Figure 2.2: Rendering of T_2-W-MRI prostate image with both 1.5 and 3.0 Tesla MRI scanner.

This modality relies on a sequence based on setting a long repetition time (TR), reducing the T_1 effect in nuclear magnetic resonance (NMR) signal measured, and fixing the echo time (TE) to sufficiently large values in order to enhance the T_2 effect of tissues. Thus, PZ and CG tissues are well perceptible in these images. The former is characterized by an intermediate/high-SI while the latter is depicted by a low-SI (5). An example of a healthy prostate is shown in Fig. 2.2(a).

In PZ, round or ill-defined low-SI masses are synonymous with CaPs (57) as shown in Fig. 2.2(b). Detecting CaP in CG is more challenging. In fact both normal CG tissue and malignant tissue, have a low-SI in T_2-W MRI reinforcing difficulties to distinguish between them. However, CaPs in CG appear often as homogeneous mass possessing ill-defined edges with lenticular or "water-drop" shapes (31, 63) as depicted in Fig. 2.2(c).

CaP aggressiveness was shown to be inversely correlated with SI. Indeed, CaPs assessed with a GS of 4-5 implied lower SI than the one with a GS of 2-3 (64).

In spite of the availability of these useful and encouraging features, the T_2-W modality lacks reliability (30, 65). Sensitivity is affected by the difficulties in detecting cancers in CG (65) while specificity rate is highly affected by outliers (31). In fact, various conditions emulate patterns of CaP such as BPH, post-biopsy haemorrhage, atrophy, scars

and post-treatment (5, 31, 60, 66, 67). These issues can be partly addressed using more innovative and advanced modalities.

2.2.2 T_2 map

As previously mentioned, T_2-W MRI modality shows low sensitivity. Moreover, T_2-W MRI images are a composite of multiple effects (56). However, T_2 values alone have been shown to be more discriminative (68) and highly correlated with citrate concentration, a biological marker in CaP (69, 70).

T_2 values are computed using the characteristics of transverse relaxation which is formalized as:

$$M_{x,y}(t) = M_{x,y}(0) \exp\left(-\frac{t}{\mathrm{T}_2}\right) \ , \tag{2.1}$$

where $M_{x,y}(0)$ is the initial value of $M_{x,y}(t)$ and T_2 is the relaxation time. By rearranging Eq. 2.1, T_2 map is computed performing a linear fitting on the model in Eq. 2.2 using several TE, $t = \{\mathrm{TE}_1, \mathrm{TE}_2, \ldots, \mathrm{TE}_m\}$.

$$\ln\left[\frac{M_{x,y}(t)}{M_{x,y}(0)}\right] = -\frac{t}{\mathrm{T}_2} \ . \tag{2.2}$$

The Fast Spin-Echo (FSE) sequence has been shown to be particularly well suited in order to build a T_2 map and obtain accurate T_2 values (71). Similar to T_2-W MRI, T_2 values associated with CaP are significantly lower than those of healthy tissues (69, 72).

2.2.3 DCE MRI

DCE MRI is an imaging technique which exploits the vascularity characteristic of tissues. Contrast media, usually gadolinium-based, is injected intravenously into the patient. The media extravasates from vessels to extravascular-extracellular space (EES) and is released back into the vasculature before being eliminated by the kidneys (73). Furthermore, the diffusion speed of the contrast agent may vary due to several parameters: (i) the permeability of the micro-vessels, (ii) their surface area and (iii) the blood flow (74).

Healthy PZ is mainly made up of glandular tissue, around 70 % (1)), which implies a reduced interstitial space restricting exchanges between vessels and EES (75, 76). Normal CG has a more disorganised structure, composed of mainly fibrous tissue (1, 30), which

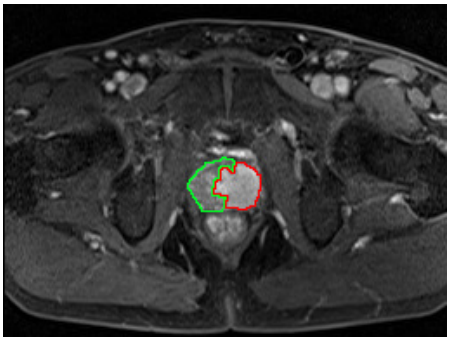

(a) T_1-W-MRI image where the cancer is delimited by the red contour. The green area was still not invaded by the CaP

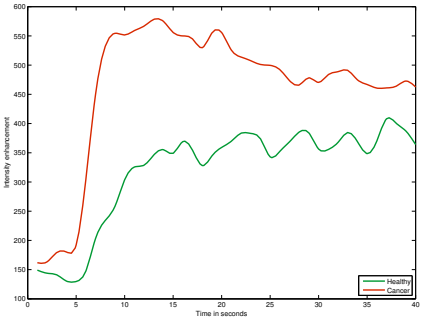

(b) Enhancement curve computed during the DCE-MRI analysis. The red curve is typical from CaP cancer while the green curve is characteristic of healthy tissue.

Figure 2.3: Illustration of typical enhancement signal observed in DCE-MRI analysis collected with a 3.0 Tesla MRI scanner.

facilitates the arrival of the contrast agent in EES (77). To understand the difference between contrast media kinetic in malignant tumours and the two previous behaviours mentioned, one has to focus on the process known as angiogenesis (78). In order to ensure growth, malignant tumours produce and release angiogenic promoter substances (78). These molecules stimulate the creation of new vessels towards the tumour (78). However, the new vessel networks in tumours differ from those present in healthy tissue (73). They are more porous due to the fact that their capillary walls have a large number of "openings" (1, 73). In contrast to healthy cases, this increased vascular permeability results in increased contrast agent exchanges between vessels and EES (79).

By making use of the previous aspects, DCE MRI is based on an acquisition of a set of T_1-W MRI images over time. The Gadolinium-based contrast agent shortens T_1 relaxation time enhancing contrast in T_1-W MRI images. The aim is to post-analyse the pharmacokinetic behaviour of the contrast media concentration in prostate tissues (79). The image analysis is carried out in two dimensions: (i) in the spatial domain on a pixel-by-pixel basis and (ii) in the time domain corresponding to the consecutive images acquired with the MRI. Thus, for each spatial location, a signal linked to contrast media concentration is measured as shown in Fig. 2.3(b) (80).

By taking the previous remarks regarding medical aspects and signal theory into

account, CaPs are characterized by a signal having an earlier and faster enhancement and an earlier wash-out (cf., the rate of the contrast agent flowing out of the tissue) (see Fig. 2.3(b)) (79). Three different approaches exist to analyse these signals with the aim of tagging them as corresponding to either normal or malignant tissues. Qualitative analysis is based on assessment of the signal shape (30).

Quantitative approaches consist of inferring pharmocokinetic parameter values (80). Those parameters are part of mathematical-pharmacokinetic models which are directly based on physiological exchanges between vessels and EES. Several pharmacokinetic models were proposed such as the Kety model (81), the Tofts model (82) and mixed models (83, 84). The last family of methods mixed both approaches and are grouped together under the heading of semi-quantitative methods. They rely on shape characterization using mathematical modelling to extract a set of parameters such as wash-in gradient, wash-out, integral under the curve, maximum signal intensity, time-to-peak enhancement and start of enhancement. These parameters will be discussed in a later section (see Fig. **??**) (30, 79). It was shown that semi-quantitative and quantitative methods improve localization of CaP when compared with qualitative methods (85). Section **??** provides a full description of quantitative and semi-quantitative approaches.

DCE MRI combined with T_2-W MRI has shown to enhance sensitivity compared to T_2-W MRI alone (86, 87, 88, 89). Despite this fact, DCE MRI possesses some drawbacks. Due to its "dynamic" nature, patient motions during the image acquisition lead to spatial misregistration of the image set (79)). Furthermore, it has been suggested that malignant tumours are difficult to distinguish from prostatitis located in PZ and BPH located in CG (30, 79). These pairs of tissues tend to have similar appearances. Later studies have shown that CaPs in CG do not always manifest in homogeneous fashion. Indeed, tumours in this zone can present both hypo-vascularization and hyper-vascularization which illustrates the challenge of CaP detection in CG (77).

2.2.4 DW MRI

As previously mentioned in the introduction, DW MRI is the most recent MRI imaging technique aiming at CaP detection and diagnosis (60). This modality exploits the variations in the motion of water molecules in different tissues (90, 91).

From a physiological point of view, the following facts can be claimed. On the one hand, PZ, as previously mentioned, is mainly glandular and tubular in structure allowing

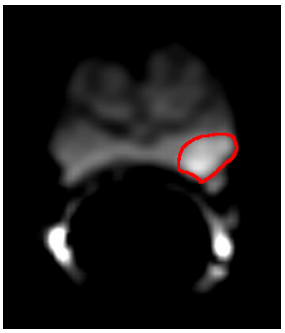

(a) DW-MRI image acquired with a 1.5 Tesla MRI scanner. The cancer corresponds to the high SI region highlighted in red.

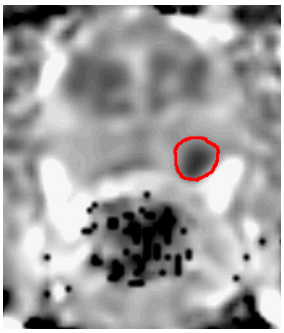

(b) ADC map computer after acquisition of DW-MRI iages with a 1.5 Tesla MRI scanner. The cancer corresponds to the low SI region highlighted in red.

Figure 2.4: Illustration of of DW-MRI and ADC map. The signal intensity corresponding to cancer are inversely correlated on these two types of imaging techniques.

water molecules to move freely (1, 30). On the other hand, CG is made up of muscular or fibrous tissue causing the motion of the water molecules to be more constrained and heterogeneous than in PZ (30). Then, CaP growth leads to the destruction of normal glandular structure and is associated with an increase in cellular density (30, 91, 92). Furthermore, these factors both have been shown to be inversely correlated with water diffusion (91, 92): higher cellular density implies a restricted water diffusion. Thus, water diffusion in CaP will be more restricted than both healthy PZ and CG (30, 91).

From the NMR principle side, DW MRI sequence produces contrasted images due to variation of water molecules motion. The method is based on the fact that the signal in DW MRI images is inversely correlated to the degree of random motion of water molecules (93). In fact, gradients are used in DW MRI modality to encode spatial location of nuclei temporarily. Simplifying the problem in only one direction, a gradient is applied in that direction, dephasing the spins of water nuclei. Hence, the spin phases vary along the gradient direction depending of the gradient intensity at those locations. Then, a second gradient is applied aiming at cancelling the spin dephasing. Thus, the immobile water molecules will be subject to the same gradient intensity as the initial one while moving water molecules will be subject to a different gradient intensity. Thus, spins

of moving water molecules will stay dephased whereas spins of immobile water molecules will come back in phase. As a consequence, a higher degree of random motion results in a more significant signal loss whereas a lower degree of random motion is synonymous with lower signal loss (93). Under these conditions, the MRI signal is measured as:

$$M_{x,y}(t,b) = M_{x,y}(0)\exp\left(-\frac{t}{\mathrm{T}_2}\right) S_{\mathrm{ADC}}(b)\ , \tag{2.3}$$

$$S_{\mathrm{ADC}}(b) = \exp\left(-b \times \mathrm{ADC}\right)\ , \tag{2.4}$$

where S_{ADC} refers to signal drop due to diffusion effect, ADC is the apparent diffusion coefficient and b is the attenuation coefficient depending only on gradient pulses parameters: (i) gradient intensity and (ii) gradient duration (94).

By using this formulation, image acquisition with a parameter $b = 0$ s.mm^{-2} corresponds to a T_2-W MRI acquisition. Then, increasing the attenuation coefficient b (cf., increase gradient intensity and duration) enhances the contrast in DW MRI images.

To summarize, in DW MRI images, CaPs are characterized by high-SI compared to normal tissues in PZ and CG as shown in Fig. 2.4(a) (31). However, some tissues in CG can look similar to CaP with higher SI (31).

Diagnosis using DW MRI combined with T_2-W MRI has shown a significant improvement compared with T_2-W MRI alone and provides highly contrasted images (1, 95, 96). As drawbacks, this modality suffers from poor spatial resolution and specificity due to false positive detection (1). With a view to eliminate these drawbacks, radiologists are extracting quantitative maps from DW MRI. This imaging technique is presented next.

2.2.5 ADC Map

The NMR signal measured for DW MRI images is not only affected by diffusion as shown in Eq. (2.3). However, the signal drop (Eq. (2.4)) is formulated such that the only variable is the acquisition parameter b (94). The ADC is considered as a "pure" diffusion coefficient and can be extracted to build a quantitative map.

From Eq. (2.3), it is clear that performing multiple acquisitions only varying b will not have any effect on the term $M_{x,y}(0)\exp\left(-\frac{t}{\mathrm{T}_2}\right)$. Thus, Eq. (2.3) can be rewritten

as:

$$S(b) = S_0 \exp\left(-b \times \text{ADC}\right) \ . \tag{2.5}$$

To compute the ADC map, a minimum of two acquisitions are necessary: (i) for $b_0 = 0$ s.mm^{-2} where the measured signal is equal to S_0, and (ii) $b_1 > 0$ s.mm^{-2} (typically 1000 s.mm^{-2}). Then, the ADC map can be computed as:

$$\text{ADC} = -\frac{\ln\left(\dfrac{S(b_1)}{S_0}\right)}{b_1} \ . \tag{2.6}$$

More accurate computation of the ADC map can be obtained by performing several acquisitions with different values for the parameter b and performing a semi-logarithmic linear fitting using the model presented in Eq. (2.5).

Regarding the appearance of the ADC maps, it was previously stated that by increasing the value of b, the signal of CaP tissue increases significantly. From Eq. (2.6), it can be shown that tissue appearance in the ADC map will be the inverse of DW MRI images. Then, CaP tissue is associated with low-SI whereas healthy tissue appears brighter as depicted in Fig. 2.4(b) (31).

Similar to the gain achieved by DW MRI, diagnosis using ADC map combined with T_2-W MRI significantly outperforms T_2-W MRI alone (1, 97). Moreover, it has been shown that ADC is correlated with GS (98, 99, 100).

However, some tissues of the CG zone mimic CaP with low-SI (65) and image distortion can arise due to haemorrhage (1). It has also been noted that a high variability of the ADC occurs between different patients making it difficult to define a static threshold to distinguish CaP from non-malignant tumours (1).

2.2.6 MRSI

CaP induces metabolic changes in the prostate compared with healthy tissue. Thus, CaP detection can be carried out by tracking changes of metabolite concentration in prostate tissue. MRSI is an NMR-based technique which generates spectra of relative metabolite concentration in a ROI.

In order to track changes of metabolite concentration, it is important to know which metabolites are associated with CaP. To address this question, clinical studies identified

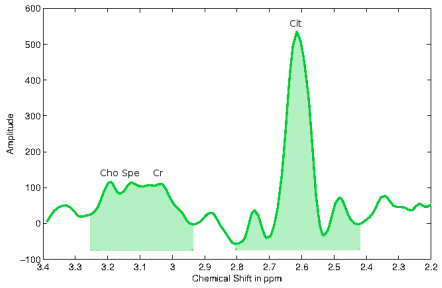

(a) Illustration of an MRSI spectrum of an healthy voxel acquired with a 3.0 Tesla MRI.

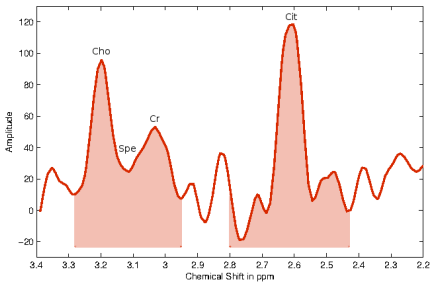

(b) Illustration of an MRSI spectrum of a cancerous voxel acquired with a 3.0 Tesla MRI.

Figure 2.5: Illustration of an MRSI spectrum both healthy and cancerous voxel with a 3.0 Tesla MRI. The highlighted areas corresponds to the related concentration of the metabolites which is computed by integrating the area under each peak. Acronyms: Choline (Cho), Spermine (Spe), Creatine (Cr) and Citrate (Cit).

three biological markers: (i) citrate, (ii) choline and (iii) polyamines composed mainly of spermine, and in less abundance of spermidine and putrescine (101, 102, 103).

Citrate is involved in the production and secretion of the prostatic fluid, and the glandular prostate cells are associated with a high production of citrate enabled by zinc accumulation by these same cells (102). However, the metabolism allowing the accumulation of citrate requires a large amount of energy (102). In contrast, malignant cells do not have high zinc levels leading to lower citrate levels due to citrate oxydation (102). Furthermore, this change results in a more energy-efficient metabolism enabling malignant cells to grow and spread (102).

An increased concentration of choline is related to CaP (101). Malignant cell development requires epigenetic mechanisms resulting in metabolic changes and relies on two mechanisms: DNA methylation and phospholid metabolism which both result in choline uptake, explaining its increased level in CaP tissue (101). Spermine is also considered as a biological marker in CaP (103, 104). In CaP, reduction of the ductal volume due to shifts in polyamine homeostasis might lead to a reduced spermine concentration (104).

To determine the concentration of these biological markers, one has to focus on the MRSI modality. In theory, in presence of a homogeneous magnetic field, identical nuclei precesses at the same operating frequency known as the Lamor frequency (105). However, MRSI is based on the fact that identical nuclei will slightly precess at different

frequencies depending on the chemical environment in which they are immersed (105), a phenomenon known as the chemical shift effect (CSE) (3). Given this property, metabolites can be identified and their concentrations can be determined. In this regard, the Fourier transform is used to obtain the frequency spectrum of the NMR signal (3, 105). In this spectrum, each peak is associated with a particular metabolite and the area under each peak corresponds to the relative concentration of this metabolite (see Fig. 2.5) (3).

Two different quantitative approaches are used to decide or whether not the spectra of a ROI is associated with CaP classified either as relative quantification or absolute quantification (106). In relative quantification, the ratio of choline-polyamines-creatine to citrate is computed. The integral of the signal is computed from choline (cf., 3.21 ppm) to creatine (cf., 3.02 ppm) because the peaks in this region can be merged at clinical magnetic field strengths (see Fig. 2.5) (30, 104). Considering the previous assumption that choline concentration rises and citrate concentration decreases in the presence of CaP, the ratio computed should be higher in malignant tissue than in healthy tissue.

Two different quantitative approaches are used to decide or not the spectra of a ROI is associated with CaP classified either as relative quantification or absolute quantification (106). In relative quantification, the ratio of choline-polyamines-creatine to citrate is computed. The integral of the signal is computed from choline (cf., 3.21 ppm) to creatine (cf., 3.02 ppm) because the peaks in this region can be merged at clinical magnetic field strengths (see Fig. 2.5) (30, 104). Considering the previous assumption that choline concentration rises and citrate concentration decreases in the presence of CaP, the ratio computed should be higher in malignant tissue than in healthy tissue.

In contrast with relative quantification, absolute quantification measures molar concentrations by normalizing relative concentrations using water as reference (106). In this case, "true" concentrations are directly used to differentiate malignant from healthy tissue. However, this method is not commonly used as it requires an additional step of acquiring water signals, inducing time and cost acquisition constraints.

MRSI allows examination with high specificity and sensitivity compared to other MRI modalities (1)). Furthermore, it has been shown that combining MRSI with MRI improves detection and diagnosis performance (107, 108, 109). Citrate and spermine concentrations are inversely correlated with the GS allowing us to distinguish low from high grade CaPs (103). However, choline concentration does not provide the same properties (103).

Unfortunately, MRSI also presents several drawbacks. First, MRSI acquisition is time consuming which prevents this modality from being used in daily clinical practise (31). In addition, MRSI suffers from low spatial resolution due to the fact that signal-to-noise (SNR) is linked to the voxel size. However, this issue is addressed by developing new scanners with higher magnetic field strengths such as 7.5 T (103). Finally, a high variability of the relative concentrations between patients was observed (1). The same observation was made depending on the zones studied (cf., PZ, CG, base, mid-gland, apex) (106, 110). Due to this variability, it is difficult to use a fixed thresholds in order to differentiate CaP from healthy tissue.

Chapter 3

Review of CADe and CADx for CaP

As previously mentioned in the introduction (see Sect. 1.4), CADs are developed to advise and backup radiologists in their tasks of CaP detection and diagnosis, but not to provide fully automatic decisions (50). CADs can be divided into two different subgroups either as CADe, with the purpose to highlight probable lesions in MRI images, or CADx, which focuses on differentiating malignant from non-malignant tumours (50). Moreover, an intuitive approach, motivated by developing a framework combining detection-diagnosis, is to mix both CADe and CADx by using the output of the former mentioned as a input of the latter named. Although the outcomes of these two systems should differ, the framework of both CAD systems is similar. A general CAD work-flow is presented n Fig. **??**. MRI modalities mentioned in Sect. **??** are used as inputs of CAD for CaP. It can be noted that ADC map is not considered as an input since it is a feature derived from the DW MRI images. The images acquired from the different modalities show a large variability between patients: the prostate organ can be located at different positions in images (e.g., patient motion, variation of acquisition plan), and the SI can be corrupted with noise or artefacts during the acquisition process (eg., magnetic field inhomogeneity, use of endorectal coil). To address these issues, the first stage of CAD is to pre-process multiparametric MRI images to reduce noise, remove artefacts and standardize the SI. Then, it is important to mention that most of the later processes would be only focused on the prostate. Thus, it is necessary to segment the prostate in each MRI-modality to define it as a ROI. However, data suffers of misalignment due to

patient motions or different acquisition plan. Therefore, a registration step is performed so that all the previously segmented MRI images will be in the same reference frame.

Some studies do not fully apply the methodology depicted in Fig. **??**. Details about those can be found in Tab. **??**. Some studies preferred to work directly with raw data in order to demonstrate the robustness of their approaches to noise or artefacts. In some cases, prostate segmentation is performed manually as well as registration. It is also sometimes assumed that no patient motions occur during the acquisition procedure, removing the need of registering the multiparametric MRI images.

Once the data are regularized, it becomes possible to extract features and classify the data to obtain the probabilistic maps. We refereed this stage to image classification where CADe and CADx are the main components.

In a CADe framework, possible lesions will be segmented automatically and further used as input of CADx. We also included in CADe studies, the methods using voxel-based delineation in which the final results will highlight the boundaries of the lesions. On the other hand, manual lesions segmentation are not considered to be part of a CADe. The output of the CADe is used as input of the CADx.

CADx is composed of the processes allowing to distinguish malignant from non-malignant tumours. We divided CADx into three different stages. First, salient features are extracted, in an pixel-based or region-based manner, from MRI images to characterize the lesion. Of course, more discriminative features will be associated with a robust and accurate likelihood cancer map. Frequently, the number of features extracted can be large resulting in redundant or insufficient discriminative features which will negatively affect the performances of the further classification. Therefore, a step consists of selecting the best features or/and reducing the number of dimensions is commonly used. Then, this modified feature vector is finally classified using different pattern recognition approaches.

As pointed out in the introduction, performance of CaP detection and diagnosis are affected by observer interpretation and limitations (50, 51). CAD offers a possible solution in order to reduce this variability. As mentioned in the introduction, the effects of CAD on the observer performance has been studied (51), with results showing that CADs benefit to less-experienced radiologist to perform similarly as experienced radiologist in their tasks (51).

3.1 Literature classification

Table 3.1: Overview of the different studies reviewed with their main characteristics. Acronyms: number (#) - image regularization (Img. Reg.).

3black!5white

Index	Study	# patients	MRI-modality				Strength of field		Studied zones		CAD stages		
			T_2-W MRI	DCE MRI	DW MRI	MRSI	1.5 T	3.0 T	PZ	CG	Img. Reg.	CADe	CADx
[1]	(?)	25	✓	✓	✗	✗	✓	✗	✓	✗	✓!	✗	✓
[2]	(?)	25	✓	✓	✗	✗	✓	✗	✓	✗	✓!	✗	✓
[3]	(?)	53	✓	✗	✓	✗	✓	✗	✓	✓	✗	✗	✓
[4]	(?)	10	✓	✓	✓	✗	✓	✗	✓	✗	✗	✓	✓
[5]	(?)	21	✓	✓	✓	✗	✓	✗	✓	✗	✓!	✓	✓
[6]	(?)	15	✓	✗	✓	✗	✓	✗	✓	✗	✗	✗	✓
[7]	(?)	10	✓	✓	✓	✗	✓	✗	✓	✗	✓	✓	✓
[8]	(?)	24	✗	✗	✗	✓	✓	✗	✓	✓	✓!	✓	✓
[9]	(?)	25	✓	✓	✓	✗	✓	✗	✓	✗	✓!	✗	✓
[10]	(?)	188	✓	✓	✓	✗	✗	✓	✓	✗	✓!	✓	✓
[11]	(?)	288	✓	✓	✓	✗	✗	✓	✓	✓	✓!	✓	✓
[12]	(?)	11	✓	✓	✓	✗	✓	✗	✓	✗	✓!	✓	✓
[13]	(?)	54	✓	✓	✓	✗	✗	✓	✓	✓	✓!	✗	✓
[14]	(?)	27	✓	✗	✗	✗	✓	✗	✓	✗	✓!	✓	✓
[15]	(?)	55	✓	✗	✗	✗	✓	✗	✓	✗	✓!	✗	✓
[16]	(?)	18	✗	✗	✗	✓	✗	✓	✓	✓	✗	✓	✓
[17]	(?)	10	✗	✓	✗	✗	✓	✗	✓	✗	✓!	✓	✓
[18]	(?)	23	✓	✓	✓	✗	✓	✗	✓	✗	✓!	✗	✓
[19]	(?)	30	✓	✓	✓	✗	✓	✗	✓	✗	✓!	✗	✓
[20]	(?)	20	✓	✓	✓	✗	✓	✗	✓	✗	✓!	✓	✓
[21]	(?)	20	✓	✓	✓	✗	✓	✗	✓	✗	✓!	✓	✓
[22]	(?)	22	✗	✗	✗	✓	✗	✓	✓	✓	✓!	✓	✓
[23]	(100)	48	✓	✓	✓	✗	✗	✓	✓	✓	✗	✗	✓
[24]	(?)	100	✗	✓	✗	✗	✓	✗	✓	✓	✗	✗	✓
[25]	(?)	42	✗	✓	✗	✗	✗	✓	✓	✓	✗	✓	✓
[26]	(?)	14	✗	✗	✗	✓	✓	✗	✓	✓	✓!	✓	✓
[27]	(?)	18	✗	✗	✗	✓	✓	✗	✓	✓	✓!	✓	✓
[28]	(?)	18	✗	✗	✗	✓	✓	✗	✓	✓	✓!	✓	✓
[29]	(?)	15	✓	✗	✗	✓	✓	✗	✓	✓	✓!	✓	✓
[30]	(?)	19	✓	✗	✗	✓	✓	✗	✓	✓	✓!	✓	✓
[31]	(?)	36	✓	✗	✗	✓	✓	✗	✓	✓	✗	✓	✓
[32]	(?)	29	✓	✗	✗	✓	✓	✗	✓	✓	✓!	✓	✓
[33]	(?)	16	✓	✗	✗	✓	✓	✗	✓	✓	✗	✓	✓
[34]	(?)	6	✓	✓	✗	✗	✗	✓	✓	✓	✓!	✓	✓
[35]	(?)	6	✓	✓	✗	✗	✗	✓	✓	✓	✓	✓	✓
[36]	(?)	12	✓	✓	✓	✗	✗	✓	✓	✓	✓!	✓	✓
[37]	(?)	22	✓	✗	✗	✗	✗	✓	✓	✓	✓	✓	✓
[38]	(?)	29	✓	✓	✗	✗	✓	✗	✓	✗	✓!	✗	✓
[39]	(?)	29	✗	✓	✗	✗	✓	✗	✓	✗	✓!	✗	✓
[40]	(?)	29	✓	✓	✗	✗	✓	✗	✓	✗	✓!	✗	✓

The CAD review is organized using the methodology presented in Fig. **??**. Methods embedded in the image regularization framework are presented before to focus on the image classification framework, the later being divided into CADe and CADx. Table **??** summarizes the different CAD studies reviewed in this paper. Characteristics related to MRI acquisition as well as CAD strategies are reported. Only methods used in CAD system are discussed.

References

[1] Y. J. Choi, J. K. Kim, N. Kim, K. W. Kim, E. K. Choi, and K. S. Cho. **Functional MR imaging of prostate cancer**. *Radiographics*, **27**:63–75, 2007. 2, 11, 12, 14, 15, 16, 18, 19

[2] K. H. Leissner and L. E. Tisell. **The weight of the human prostate**. *Scand. J. Urol. Nephrol.*, **13**(2):137–142, 1979. 1

[3] S. Parfait. *Classification de spectres et recherche de biomarqueurs en spectroscopie par résonqnce magnétique nulcléaire du proton dans les tumeurs prostatiques*. PhD thesis, Université de Bourgogne, 2010. 1, 3, 4, 18

[4] J. E. McNeal. **The zonal anatomy of the prostate**. *Prostate*, **2**:35–49, 1981. 1

[5] H. Hricak, G. C. Dooms, J. E. McNeal, A. S. Mark, M. Marotti, A. Avallone, M. Pelzer, E. C. Proctor, and E. A. Tanagho. **MR imaging of the prostate gland: normal anatomy**. *AJR Am J Roentgenol*, **148**:51–58, Jan 1987. 2, 10, 11

[6] A. Villers, A. Steg, and L. Boccon-Gibod. **Anatomy of the prostate: review of the different models**. *Eur. Urol.*, **20**:261–268, 1991. 2

[7] F. V. Coakley and H. Hricak. **Radiologic anatomy of the prostate gland: a clinical approach**. *Radiol. Clin. North Am.*, **38**:15–30, Jan 2000. 2

[8] J. Ferlay, H. R. Shin, F. Bray, D. Forman, C. Mathers, and D. M. Parkin. **Estimates of worldwide burden of cancer in 2008: GLOBOCAN 2008**. *Int. J. Cancer*, **127**(12):2893–2917, Dec 2010. 2

[9] R. Siegel, D. Naishadham, and A. Jemal. **Cancer statistics, 2013**. *CA Cancer J Clin*, **63**(1):11–30, Jan 2013. 3

[10] A. C. American Cancer Society. **Cancer Facts and Figures 2013**. http://www.cancer.org/research/cancerfactsfigures, 2013. Accessed: 2013-08-01. 3

[11] A. C. American Cancer Society. **Cancer Facts and Figures 2010**. http://www.cancer.org/research/cancerfactsfigures, 2010. Accessed: 2013-08-01. 3

[12] E. Giovannucci, Y. Liu, E. A. Platz, M. J. Stampfer, and W. C. Willett. **Risk factors for prostate cancer incidence and progression in the health professionals follow-up study**. *Int. J. Cancer*, **121**(7):1571–1578, Oct 2007. 3

[13] G. D. Steinberg, B. S. Carter, T. H. Beaty, B. Childs, and P. C. Walsh. **Family history and the risk of prostate cancer**. *Prostate*, **17**(4):337–347, 1990. 3

[14] M. L. Freedman, C. A. Haiman, N. Patterson, G. J. McDonald, A. Tandon, A. Waliszewska, K. Penney, R. G. Steen, K. Ardlie, E. M. John, I. Oakley-Girvan, A. S. Whittemore, K. A. Cooney, S. A. Ingles, D. Altshuler, B. E. Henderson, and D. Reich. **Admixture mapping identifies 8q24 as a prostate cancer risk locus in African-American men**. *Proc. Natl. Acad. Sci. U.S.A.*, **103**(38):14068–14073, Sep 2006. 3

[15] L. T. Amundadottir, P. Sulem, J. Gudmundsson, A. Helgason, A. Baker, B. A. Agnarsson, A. Sigurdsson, K. R. Benediktsdottir, J. B. Cazier, J. Sainz, M. Jakobsdottir, J. Kostic, D. N. Magnusdottir, S. Ghosh, K. Agnarsson, B. Birgisdottir, L. Le Roux, A. Olafsdottir, T. Blondal, M. Andresdottir, O. S. Gretarsdottir, J. T. Bergthorsson, D. Gudbjartsson, A. Gylfason, G. Thorleifsson, A. Manolescu, K. Kristjansson, G. Geirsson, H. Isaksson, J. Douglas, J. E. Johansson, K. Balter, F. Wiklund, J. E. Montie, X. Yu, B. K. Suarez, C. Ober, K. A. Cooney, H. Gronberg, W. J. Catalona, G. V. Einarsson, R. B. Barkardottir, J. R. Gulcher, A. Kong, U. Thorsteinsdottir, and K. Stefansson. **A common variant associated with prostate cancer in European and African populations**. *Nat. Genet.*, **38**(6):652–658, Jun 2006. 3

[16] I. Agalliu, R. Gern, S. Leanza, and R. D. Burk. **Associations of high-grade prostate cancer with BRCA1 and BRCA2 founder mutations**. *Clin. Cancer Res.*, **15**(3):1112–1120, Feb 2009. 3

[17] R. M. Hoffman, F. D. Gilliland, J. W. Eley, L. C. Harlan, R. A. Stephenson, J. L. Stanford, P. C. Albertson, A. S. Hamilton, W. C. Hunt, and A. L. Potosky. **Racial and ethnic differences in advanced-stage prostate cancer: the Prostate Cancer Outcomes Study**. *J. Natl. Cancer Inst.*, **93**(5):388–395, Mar 2001. 3

[18] R. W. Ma and K. Chapman. **A systematic review of the effect of diet in prostate cancer prevention and treatment**. *J Hum Nutr Diet*, **22**(3):187–199, Jun 2009. 3

[19] D. D. Alexander, P. J. Mink, C. A. Cushing, and B. Sceurman. **A review and meta-analysis of prospective studies of red and processed meat intake and prostate cancer**. *Nutr J*, **9**:50, 2010. 3

[20] C. Rodriguez, S. J. Freedland, A. Deka, E. J. Jacobs, M. L. McCullough, A. V. Patel, M. J. Thun, and E. E. Calle. **Body mass index, weight change, and risk of prostate cancer in the Cancer Prevention Study II Nutrition Cohort**. *Cancer Epidemiol. Biomarkers Prev.*, **16**(1):63–69, Jan 2007. 3

[21] S.B. Strum and D. Pogliano. **What every doctor who treats male patients should know**. PCRI Insights vol. 8, no. 2, May 2005. 3

[22] G. L. Lu-Yao, P. C. Albertsen, D. F. Moore, W. Shih, Y. Lin, R. S. DiPaola, M. J. Barry, A. Zietman, M. O'Leary, E. Walker-Corkery, and S. L. Yao. **Outcomes of localized prostate cancer following conservative management**. *JAMA*, **302**(11):1202–1209, Sep 2009. 3

REFERENCES

[23] G. Oster, L. Lamerato, A. G. Glass, K. E. Richert-Boe, A. Lopez, K. Chung, A. Richhariya, T. Dodge, G. G. Wolff, A. Balakumaran, and J. Edelsberg. **Natural history of skeletal-related events in patients with breast, lung, or prostate cancer and metastases to bone: a 15-year study in two large US health systems**. *Support Care Cancer*, **21**(12):3279–3286, Dec 2013. 3

[24] L. Ye, H. G. Kynaston, and W. G. Jiang. **Bone metastasis in prostate cancer: molecular and cellular mechanisms (Review)**. *Int. J. Mol. Med.*, **20**(1):103–111, Jul 2007. 3

[25] C. L. Carrol, F. G. Sommer, J. E. McNeal, and T. A. Stamey. **The abnormal prostate: MR imaging at 1.5 T with histopathologic correlation**. *Radiology*, **163**(2):521–525, May 1987. 3

[26] J. E. McNeal, E. A. Redwine, F. S. Freiha, and T. A. Stamey. **Zonal distribution of prostatic adenocarcinoma. Correlation with histologic pattern and direction of spread**. *Am. J. Surg. Pathol.*, **12**(12):897–906, Dec 1988. 3

[27] T. A. Stamey, A. N. Donaldson, C. E. Yemoto, J. E. McNeal, S. Sozen, and H. Gill. **Histological and clinical findings in 896 consecutive prostates treated only with radical retropubic prostatectomy: epidemiologic significance of annual changes**. *J. Urol.*, **160**(6 Pt 2):2412–2417, Dec 1998. 3

[28] R. J. Cohen, B. A. Shannon, M. Phillips, R. E. Moorin, T. M. Wheeler, and K. L. Garrett. **Central zone carcinoma of the prostate gland: a distinct tumor type with poor prognostic features**. *J. Urol.*, **179**(5):1762–1767, May 2008. 3

[29] R. Etzioni, D. F. Penson, J. M. Legler, D. di Tommaso, R. Boer, P. H. Gann, and E. J. Feuer. **Overdiagnosis due to prostate-specific antigen screening: lessons from U.S. prostate cancer incidence trends**. *J. Natl. Cancer Inst.*, **94**(13):981–990, Jul 2002. 3

[30] C. M. Hoeks, J. O. Barentsz, T. Hambrock, D. Yakar, D. M. Somford, S. W. Heijmink, T. W. Scheenen, P. C. Vos, H. Huisman, I. M. van Oort, J. A. Witjes, A. Heerschap, and J. J. Futterer. **Prostate cancer: multiparametric MR imaging for detection, localization, and staging**. *Radiology*, **261**(1):46–66, Oct 2011. 3, 4, 10, 11, 13, 14, 18

[31] J. O. Barentsz, J. Richenberg, R. Clements, P. Choyke, S. Verma, G. Villeirs, O. Rouviere, V. Logager, and J. J. Futterer. **ESUR prostate MR guidelines 2012**. *Eur Radiol*, **22**(4):746–757, Apr 2012. 4, 7, 10, 11, 15, 16, 19

[32] D. F. Gleason. *Urologic pathology: The prostate*, chapter The Veteran's Administration Cooperative Urologic Research Group: histologic grading and clinical staging of prostatic carcinoma, page 171198. Lea and Febiger., 1977. 4

[33] J. I. Epstein, W. C. Allsbrook, M. B. Amin, and L. L. Egevad. **The 2005 International Society of Urological Pathology (ISUP) Consensus Conference on Gleason Grading of Prostatic Carcinoma**. *Am. J. Surg. Pathol.*, **29**(9):1228–1242, Sep 2005. 4

[34] N. Hara, M. Okuizumi, H. Koike, M. Kawaguchi, and V. Bilim. **Dynamic contrast-enhanced magnetic resonance imaging (DCE-MRI) is a useful modality for the precise detection and staging of early prostate cancer**. *Prostate*, **62**(2):140–147, Feb 2005. 4

[35] R. Chou, J. M. Croswell, T. Dana, C. Bougatsos, I. Blazina, R. Fu, K. Gleitsmann, H. C. Koenig, C. Lam, A. Maltz, J. B. Rugge, and K. Lin. **Screening for prostate cancer: a review of the evidence for the U.S. Preventive Services Task Force**. *Ann. Intern. Med.*, **155**(11):762–771, Dec 2011. 4

[36] Gerald L. Andriole, E. David Crawford, Robert L. Grubb, Saundra S. Buys, David Chia, Timothy R. Church, Mona N. Fouad, Edward P. Gelmann, Paul A. Kvale, Douglas J. Reding, Joel L. Weissfeld, Lance A. Yokochi, Barbara O'Brien, Jonathan D. Clapp, Joshua M. Rathmell, Thomas L. Riley, Richard B. Hayes, Barnett S. Kramer, Grant Izmirlian, Anthony B. Miller, Paul F. Pinsky, Philip C. Prorok, John K. Gohagan, and Christine D. Berg. **Mortality results from a randomized Prostate-cancer screening trial**. *New England Journal of Medicine*, **360**(13):1310–1319, 2009. 4

[37] Fritz H. Schröder, Jonas Hugosson, Monique J. Roobol, Teuvo L.J. Tammela, Stefano Ciatto, Vera Nelen, Maciej Kwiatkowski, Marcos Lujan, Hans Lilja, Marco Zappa, Louis J. Denis, Franz Recker, Alvaro Pez, Liisa Määttänen, Chris H. Bangma, Gunnar Aus, Sigrid Carlsson, Arnauld Villers, Xavier Rebillard, Theodorus van der Kwast, Paula M. Kujala, Bert G. Blijenberg, Ulf-Hakan Stenman, Andreas Huber, Kimmo Taari, Matti Hakama, Sue M. Moss, Harry J. de Koning, and Anssi Auvinen. **Prostate-cancer mortality at 11 years of follow-up**. *New England Journal of Medicine*, **366**(11):981–990, 2012. 4

[38] J. Hugosson, S. Carlsson, G. Aus, S. Bergdahl, A. Khatami, P. Lodding, C. G. Pihl, J. Stranne, E. Holmberg, and H. Lilja. **Mortality results from the Göteborg randomised population-based prostate-cancer screening trial**. *Lancet Oncol.*, **11**(8):725–732, Aug 2010. 4

[39] A. Heidenreich, P. A. Abrahamsson, W. Artibani, J. Catto, F. Montorsi, H. Van Poppel, M. Wirth, and N. Mottet. **Early detection of prostate cancer: European Association of Urology recommendation**. *Eur. Urol.*, **64**(3):347–354, Sep 2013. 4

[40] F. H. Schroder, H. B. Carter, T. Wolters, R. C. van den Bergh, C. Gosselaar, C. H. Bangma, and M. J. Roobol. **Early detection of prostate cancer in 2007. Part 1: PSA and PSA kinetics**. *Eur. Urol.*, **53**(3):468–477, Mar 2008. 4

[41] C. Delpierre, S. Lamy, M. Kelly-Irving, F. Molinie, M. Velten, B. Tretarre, A. S. Woronoff, A. Buemi, B. Lapotre-Ledoux, S. Bara, A. V. Guizard, M. Colonna, and P. Grosclaude. **Life expectancy estimates as a key factor in over-treatment: the case of prostate cancer**. *Cancer Epidemiol*, **37**(4):462–468, Aug 2013. 4

[42] A. Bourdoumis, A. G. Papatsoris, M. Chrisofos, E. Efstathiou, A. Skolarikos, and C. Deliveliotis. **The novel prostate cancer antigen 3 (PCA3) biomarker**. *Int Braz J Urol*, **36**(6):665–668, 2010. 4

[43] R. Morgan, A. Boxall, A. Bhatt, M. Bailey, R. Hindley, S. Langley, H. C. Whitaker, D. E. Neal, M. Ismail, H. Whitaker, N. Annels, A. Michael, and H. Pandha. **Engrailed-2 (EN2): a tumor specific urinary biomarker for the early diagnosis of prostate cancer**. *Clin. Cancer Res.*, **17**(5):1090–1098, Mar 2011. 4

[44] J.Chad Brenner, ArulM. Chinnaiyan, and ScottA. Tomlins. **ETS fusion genes in prostate cancer**. In Donald J. Tindall, editor, *Prostate Cancer*, **16** of *Protein Reviews*, pages 139–183. Springer New York, 2013. 4

[45] C. M. Moore, A. Ridout, and M. Emberton. **The role of MRI in active surveillance of prostate cancer**. *Curr Opin Urol*, **23**(3):261–267, May 2013. 4

[46] M. Noguchi, T. A. Stamey, J. E. McNeal, and C. M. Yemoto. **Relationship between systematic biopsies and histological features of 222 radical prostatectomy specimens: lack of prediction of tumor significance for men with nonpalpable prostate cancer**. *J. Urol.*, **166**(1):104–109, Jul 2001. 5

[47] G. P. Haas, N. B. Delongchamps, R. F. Jones, V. Chandan, A. M. Serio, A. J. Vickers, M. Jumbelic, G. Threatte, R. Korets, H. Lilja, and G. de la Roza. **Needle biopsies on autopsy prostates: sensitivity of cancer detection based on true prevalence**. *J. Natl. Cancer Inst.*, **99**(19):1484–1489, Oct 2007. 5

[48] A. V. Taira, G. S. Merrick, R. W. Galbreath, H. Andreini, W. Taubenslag, R. Curtis, W. M. Butler, E. Adamovich, and K. E. Wallner. **Performance of transperineal template-guided mapping biopsy in detecting prostate cancer in the initial and repeat biopsy setting**. *Prostate Cancer Prostatic Dis.*, **13**(1):71–77, Mar 2010. 5

[49] N. B. Delongchamps, M. Peyromaure, A. Schull, F. Beuvon, N. Bouazza, T. Flam, M. Zerbib, N. Muradyan, P. Legman, and F. Cornud. **Prebiopsy magnetic resonance imaging and prostate cancer detection: comparison of random and targeted biopsies**. *J. Urol.*, **189**(2):493–499, Feb 2013. 5

[50] M. L. Giger, H. P. Chan, and J. Boone. **Anniversary paper: History and status of CAD and quantitative image analysis: the role of Medical Physics and AAPM**. *Med Phys*, **35**(12):5799–5820, Dec 2008. 5

[51] T. Hambrock, P. C. Vos, C. A. Hulsbergen-van de Kaa, J. O. Barentsz, and H. J. Huisman. **Prostate cancer: computer-aided diagnosis with multiparametric 3-T MR imaging–effect on observer performance**. *Radiology*, **266**(2):521–530, Feb 2013. 5, 6

[52] H. P. Chan, B. Sahiner, M. A. Helvie, N. Petrick, M. A. Roubidoux, T. E. Wilson, D. D. Adler, C. Paramagul, J. S. Newman, and S. Sanjay-Gopal. **Improvement of radiologists' characterization of mammographic masses by using computer-aided diagnosis: an ROC study**. *Radiology*, **212**(3):817–827, Sep 1999. 6

[53] J. C. Dean and C. C. Ilvento. **Improved cancer detection using computer-aided detection with diagnostic and screening mammography: prospective study of 104 cancers**. *AJR Am J Roentgenol*, **187**(1):20–28, Jul 2006. 6

[54] F. Li, M. Aoyama, J. Shiraishi, H. Abe, Q. Li, K. Suzuki, R. Engelmann, S. Sone, H. Macmahon, and K. Doi. **Radiologists' performance for differentiating benign from malignant lung nodules on high-resolution CT using computer-estimated likelihood of malignancy**. *AJR Am J Roentgenol*, **183**(5):1209–1215, Nov 2004. 6

[55] N. Petrick, M. Haider, R. M. Summers, S. C. Yeshwant, L. Brown, E. M. Iuliano, A. Louie, J. R. Choi, and P. J. Pickhardt. **CT colonography with computer-aided detection as a second reader: observer performance study**. *Radiology*, **246**(1):148–156, Jan 2008. 6

[56] J. V. Hegde, R. V. Mulkern, L. P. Panych, F. M. Fennessy, A. Fedorov, S. E. Maier, and C. M. Tempany. **Multiparametric MRI of prostate cancer: an update on state-of-the-art techniques and their performance in detecting and localizing prostate cancer**. *J Magn Reson Imaging*, **37**(5):1035–1054, May 2013. 6, 11

[57] H. Hricak, R. D. Williams, D. B. Spring, K. L. Moon, M. W. Hedgcock, R. A. Watson, and L. E. Crooks. **Anatomy and pathology of the male pelvis by magnetic resonance imaging**. *AJR Am J Roentgenol*, **141**(6):1101–1110, Dec 1983. 6, 7, 10

[58] R. A. Huch Boni, J. A. Boner, U. M. Lutolf, F. Trinkler, D. M. Pestalozzi, and G. P. Krestin. **Contrast-enhanced endorectal coil MRI in local staging of prostate carcinoma**. *J Comput Assist Tomogr*, **19**(2):232–237, 1995. 6

[59] J. Kurhanewicz, D. B. Vigneron, H. Hricak, P. Narayan, P. Carroll, and S. J. Nelson. **Three-dimensional H-1 MR spectroscopic imaging of the in situ human prostate with high (0.24-0.7-cm3) spatial resolution**. *Radiology*, **198**(3):795–805, Mar 1996. 6

[60] J. Scheidler, R. Petsch, U. Muller-Lisse, A.F. Heuck, and M. Reiser. **Echo-planar diffusion-weighted MR imaging of the prostate**. In *Proceedings of the 7th Annual Meeting of ISMRM Philadelphia*, page 1103, 1999. 6, 11, 13

[61] M. G. Swanson, D. B. Vigneron, T. K. Tran, N. Sailasuta, R. E. Hurd, and J. Kurhanewicz. **Single-voxel oversampled J-resolved spectroscopy of in vivo human prostate tissue**. *Magn Reson Med*, **45**(6):973–980, Jun 2001. 6

[62] B. Turkbey and P. L. Choyke. **Multiparametric MRI and prostate cancer diagnosis and risk stratification**. *Curr Opin Urol*, **22**(4):310–315, Jul 2012. 7

[63] O. Akin, E. Sala, C. S. Moskowitz, K. Kuroiwa, N. M. Ishill, D. Pucar, P. T. Scardino, and H. Hricak. **Transition zone prostate cancers: features, detection, localization, and staging at endorectal MR imaging**. *Radiology*, **239**(3):784–792, Jun 2006. 10

[64] L. Wang, Y. Mazaheri, J. Zhang, N. M. Ishill, K. Kuroiwa, and H. Hricak. **Assessment of biologic aggressiveness of prostate cancer: correlation of MR signal intensity with Gleason grade after radical prostatectomy**. *Radiology*, **246**(1):168–176, Jan 2008. 10

[65] A. P. Kirkham, M. Emberton, and C. Allen. **How good is MRI at detecting and characterising cancer within the prostate?** *Eur. Urol.*, **50**(6):1163–1174, Dec 2006. 10, 16

[66] L. E. Quint, J. S. Van Erp, P. H. Bland, S. H. Mandell, E. A. Del Buono, H. B. Grossman, G. M. Glazer, and P. W. Gikas. **Carcinoma of the prostate: MR images obtained with body coils do not accurately reflect tumor volume**. *AJR Am J Roentgenol*, **156**(3):511–516, Mar 1991. 11

[67] M. Cruz, K. Tsuda, Y. Narumi, Y. Kuroiwa, T. Nose, Y. Kojima, A. Okuyama, S. Takahashi, K. Aozasa, J. O. Barentsz, and H. Nakamura. **Characterization of low-intensity lesions in the peripheral zone of prostate on prebiopsy endorectal coil MR imaging**. *Eur Radiol*, **12**(2):357–365, Feb 2002. 11

[68] W. Liu, B. Turkbey, J. Senegas, S. Remmele, S. Xu, J. Kruecker, M. Bernardo, B. J. Wood, P. A. Pinto, and P. L. Choyke. **Accelerated T2 mapping for characterization of prostate cancer**. *Magn Reson Med*, **65**(5):1400–1406, May 2011. 11

[69] G. P. Liney, M. Lowry, L. W. Turnbull, D. J. Manton, A. J. Knowles, S. J. Blackband, and A. Horsman. **Proton MR T2 maps correlate with the citrate concentration in the prostate**. *NMR Biomed*, **9**(2):59–64, Apr 1996. 11

[70] G. P. Liney, L. W. Turnbull, M. Lowry, L. S. Turnbull, A. J. Knowles, and A. Horsman. **In vivo quantification of citrate concentration and water T2 relaxation time of the pathologic prostate gland using 1H MRS and MRI**. *Magn Reson Imaging*, **15**(10):1177–1186, 1997. 11

[71] G. P. Liney, A. J. Knowles, D. J. Manton, L. W. Turnbull, S. J. Blackband, and A. Horsman. **Comparison of conventional single echo and multi-echo sequences with a fast spin-echo sequence for quantitative T2 mapping: application to the prostate**. *J Magn Reson Imaging*, **6**(4):603–607, 1996. 11

[72] P. Gibbs, D. J. Tozer, G. P. Liney, and L. W. Turnbull. **Comparison of quantitative T2 mapping and diffusion-weighted imaging in the normal and pathologic prostate**. *Magn Reson Med*, **46**(6):1054–1058, Dec 2001. 11

[73] IngridS. Gribbestad, KjelliI. Gjesdal, Gunnar Nilsen, Steinar Lundgren, MariH.B. Hjelstuen, and Alan Jackson. **An introduction to dynamic contrast-enhanced MRI in oncology**. In Alan Jackson, DavidL. Buckley, and GeoffreyJ.M. Parker, editors, *Dynamic Contrast-Enhanced Magnetic Resonance Imaging in Oncology*, Medical Radiology, pages 1–22. Springer Berlin Heidelberg, 2005. 11, 12

[74] A. R. Padhani. **Dynamic contrast-enhanced MRI in clinical oncology: current status and future directions**. *J Magn Reson Imaging*, **16**(4):407–422, Oct 2002. 11

[75] D. L. Buckley, C. Roberts, G. J. Parker, J. P. Logue, and C. E. Hutchinson. **Prostate cancer: evaluation of vascular characteristics with dynamic contrast-enhanced T1-weighted MR imaging–initial experience**. *Radiology*, **233**(3):709–715, Dec 2004. 11

[76] C. G. van Niekerk, J. A. van der Laak, M. E. Borger, H. J. Huisman, J. A. Witjes, J. O. Barentsz, and C. A. Hulsbergen-van de Kaa. **Computerized whole slide quantification shows increased microvascular density in pT2 prostate cancer as compared to normal prostate tissue**. *Prostate*, **69**(1):62–69, Jan 2009. 11

[77] C. G. van Niekerk, J. A. Witjes, J. O. Barentsz, J. A. van der Laak, and C. A. Hulsbergen-van de Kaa. **Microvascularity in transition zone prostate tumors resembles normal prostatic tissue**. *Prostate*, **73**(5):467–475, Apr 2013. 12, 13

[78] P. Carmeliet and R. K. Jain. **Angiogenesis in cancer and other diseases**. *Nature*, **407**(6801):249–257, Sep 2000. 12

[79] S. Verma, B. Turkbey, N. Muradyan, A. Rajesh, F. Cornud, M. A. Haider, P. L. Choyke, and M. Harisinghani. **Overview of dynamic contrast-enhanced MRI in prostate cancer diagnosis and management**. *AJR Am J Roentgenol*, **198**(6):1277–1288, Jun 2012. 12, 13

[80] P.S. Tofts. **T1-weighted DCE imaging concepts: modelling, acquisition and analysis**. In *Magneton Flash*. Siemens, 2010. 12, 13

[81] S.S. Kety. **The theory and applications of the exchange of inert gas at the lungs and tissues**. *Pharmacol. Rev.*, **3**(1):1–41, Mar 1951. 13

[82] P. S. Tofts. **Modeling tracer kinetics in dynamic Gd-DTPA MR imaging**. *J Magn Reson Imaging*, **7**(1):91–101, 1997. 13

[83] H. B. Larsson, T. Fritz-Hansen, E. Rostrup, L. Sondergaard, P. Ring, and O. Henriksen. **Myocardial perfusion modeling using MRI**. *Magn Reson Med*, **35**(5):716–726, May 1996. 13

[84] K. S. St Lawrence and T. Y. Lee. **An adiabatic approximation to the tissue homogeneity model for water exchange in the brain: I. Theoretical derivation**. *J. Cereb. Blood Flow Metab.*, **18**(12):1365–1377, Dec 1998. 13

[85] A. B. Rosenkrantz, A. Sabach, J. S. Babb, B. W. Matza, S. S. Taneja, and F. M. Deng. **Prostate cancer: comparison of dynamic contrast-enhanced MRI techniques for localization of peripheral zone tumor**. *AJR Am J Roentgenol*, **201**(3):W471–478, Sep 2013. 13

[86] G. J. Jager, E. T. Ruijter, C. A. van de Kaa, J. J. de la Rosette, G. O. Oosterhof, J. R. Thornbury, S. H. Ruijs, and J. O. Barentsz. **Dynamic TurboFLASH subtraction technique for contrast-enhanced MR imaging of the prostate: correlation with histopathologic results**. *Radiology*, **203**(3):645–652, Jun 1997. 13

[87] J. K. Kim, S. S. Hong, Y. J. Choi, S. H. Park, H. Ahn, C. S. Kim, and K. S. Cho. **Wash-in rate on the basis of dynamic contrast-enhanced MRI: usefulness for prostate cancer detection and localization**. *J Magn Reson Imaging*, **22**(5):639–646, Nov 2005. 13

[88] H. P. Schlemmer, J. Merkle, R. Grobholz, T. Jaeger, M. S. Michel, A. Werner, J. Rabe, and G. van Kaick. **Can preoperative contrast-enhanced dynamic MR imaging for prostate cancer predict microvessel density in prostatectomy specimens?** *Eur Radiol*, **14**(2):309–317, Feb 2004. 13

[89] B. Zelhof, M. Lowry, G. Rodrigues, S. Kraus, and L. Turnbull. **Description of magnetic resonance imaging-derived enhancement variables in pathologically confirmed prostate cancer and normal peripheral zone regions**. *BJU Int.*, **104**(5):621–627, Sep 2009. 13

[90] D. Le Bihan, E. Breton, D. Lallemand, M. L. Aubin, J. Vignaud, and M. Laval-Jeantet. **Separation of diffusion and perfusion in intravoxel incoherent motion MR imaging**. *Radiology*, **168**(2):497–505, Aug 1988. 13

[91] D. M. Koh and D. J. Collins. **Diffusion-weighted MRI in the body: applications and challenges in oncology**. *AJR Am J Roentgenol*, **188**(6):1622–1635, Jun 2007. 13, 14

[92] D. M. Somford, J. J. Futterer, T. Hambrock, and J. O. Barentsz. **Diffusion and perfusion MR imaging of the prostate**. *Magn Reson Imaging Clin N Am*, **16**(4):685–695, Nov 2008. 14

[93] T. A. Huisman. **Diffusion-weighted imaging: basic concepts and application in cerebral stroke and head trauma**. *Eur Radiol*, **13**(10):2283–2297, Oct 2003. 14, 15

[94] D. Le Bihan, E. Breton, D. Lallemand, P. Grenier, E. Cabanis, and M. Laval-Jeantet. **MR imaging of intravoxel incoherent motions: application to diffusion and perfusion in neurologic disorders**. *Radiology*, **161**(2):401–407, Nov 1986. 15

[95] R. Shimofusa, H. Fujimoto, H. Akamata, K. Motoori, S. Yamamoto, T. Ueda, and H. Ito. **Diffusion-weighted imaging of prostate cancer**. *J Comput Assist Tomogr*, **29**(2):149–153, 2005. 15

[96] A. R. Padhani. **Integrating multiparametric prostate MRI into clinical practice**. *Cancer Imaging*, **11 Spec No A**:27–37, 2011. 15

[97] K. W. Doo, D. J. Sung, B. J. Park, M. J. Kim, S. B. Cho, Y. W. Oh, Y. H. Ko, and K. S. Yang. **Detectability of low and intermediate or high risk prostate cancer with combined T2-weighted and diffusion-weighted MRI**. *Eur Radiol*, **22**(8):1812–1819, Aug 2012. 16

[98] T. Hambrock, D. M. Somford, H. J. Huisman, I. M. van Oort, J. A. Witjes, C. A. Hulsbergen-van de Kaa, T. Scheenen, and J. O. Barentsz. **Relationship between apparent diffusion coefficients at 3.0-T MR imaging and Gleason grade in peripheral zone prostate cancer**. *Radiology*, **259**(2):453–461, May 2011. 16

[99] Y. Itou, K. Nakanishi, Y. Narumi, Y. Nishizawa, and H. Tsukuma. **Clinical utility of apparent diffusion coefficient (ADC) values in patients with prostate cancer: can ADC values contribute to assess the aggressiveness of prostate cancer?** *J Magn Reson Imaging*, **33**(1):167–172, Jan 2011. 16

[100] Y. Peng, Y. Jiang, C. Yang, J.B. Brown, T. Antic, I. Sethi, C. Schmid-Tannwald, M.L. Giger, S.E. Eggener, and A. Oto. **Quantitative analysis of multiparametric prostate MR images: differentiation between prostate cancer and normal tissue and correlation with Gleason score–a computer-aided diagnosis development study**. *Radiology*, **267**(1):787–796, June 2013. 16

[101] H. M. Awwad, J. Geisel, and R. Obeid. **The role of choline in prostate cancer**. *Clin. Biochem.*, **45**(18):1548–1553, Dec 2012. 17

[102] L. C. Costello and R. B. Franklin. **The clinical relevance of the metabolism of prostate cancer; zinc and tumor suppression: connecting the dots**. *Mol. Cancer*, **5**:17, 2006. 17

[103] G. F. Giskeodegard, H. Bertilsson, K. M. Selnaes, A. J. Wright, T. F. Bathen, T. Viset, J. Halgunset, A. Angelsen, I. S. Gribbestad, and M. B. Tessem. **Spermine and citrate as metabolic biomarkers for assessing prostate cancer aggressiveness**. *PLoS ONE*, **8**(4):e62375, 2013. 17, 18, 19

[104] M. van der Graaf, R. G. Schipper, G. O. Oosterhof, J. A. Schalken, A. A. Verhofstad, and A. Heerschap. **Proton MR spectroscopy of prostatic tissue focused on the detection of spermine, a possible biomarker of malignant behavior in prostate cancer**. *MAGMA*, **10**(3):153–159, Jul 2000. 17, 18

[105] E.M. Haacke, R.W. Brown, M.R. Thompson, and R. Venkatesan. *Magnetic resonance imaging: Physical principles and sequence design*. Wiley, 1999. 17, 18

[106] G. Lemaître. *Absolute quantification at 3 T*. Master's thesis, Université de Bourgogne, Heriot-Watt University, Universitat de Girona, 2011. 18, 19

[107] J. Scheidler, H. Hricak, D. B. Vigneron, K. K. Yu, D. L. Sokolov, L. R. Huang, C. J. Zaloudek, S. J. Nelson, P. R. Carroll, and J. Kurhanewicz. **Prostate cancer: localization with three-dimensional proton MR spectroscopic imaging–clinicopathologic study**. *Radiology*, **213**(2):473–480, Nov 1999. 18

[108] Y. Kaji, J. Kurhanewicz, H. Hricak, D. L. Sokolov, L. R. Huang, S. J. Nelson, and D. B. Vigneron. **Localizing prostate cancer in the presence of postbiopsy changes on MR images: role of proton MR spectroscopic imaging**. *Radiology*, **206**(3):785–790, Mar 1998. 18

[109] Joan C Vilanova, Josep Comet, Carles Barceló-Vidal, Joaquim Barceló, Eugeni López-Bonet, Albert Maroto, Montse Arzoz, Àngel Moreno, and Joan Areal. **Peripheral zone prostate cancer in patients with elevated PSA levels and low free-to-total PSA ratio: detection with MR imaging and MR spectroscopy**. *Radiology*, **253**(1):135–143, 2009. 18

[110] P.M. Walker, G. Crehange, S. Parfait, A. Cochet, P. Maignon, L. Cormier, and F. Brunotte. **Absolute quantification in 1H MRSI of the prostate at 3T**. In *ISMRM Annual Meeting 2010*, 2010. 19

Declaration

I herewith declare that I have produced this paper without the prohibited assistance of third parties and without making use of aids other than those specified; notions taken over directly or indirectly from other sources have been identified as such. This paper has not previously been presented in identical or similar form to any other German or foreign examination board.

The thesis work was conducted from XXX to YYY under the supervision of PI at ZZZ.

CITY,